JOURNAL OF
EMERGING INVESTIGATORS

Simulating the Energy Harnessing Capabilities of CdSe Quantum Dots and a Comparison to Traditional Solar Cells

Rohan Shankar[1*], Krish Arora[1*], Shrey Birmiwal[1], Shankar Jayaraman[2]

[1] Westwood High School, Austin, Texas
[2] Marriott International, Baltimore, Maryland
[*] *These authors contributed equally to this work*

Student Authors
Rohan Shankar - High School
Krish Arora - High School
Shrey Birmiwal - High School

SUMMARY

Quantum dots are the future of solar energy production, promising conversion efficiencies that might one day rival or even outperform traditional solar panel technology. However, experimental development of quantum dots with the most optimal setups takes months of tedious and costly preparation. To mitigate the cost of this research, simulations of said quantum dots can be used to identify optimal parameters without the need to conduct numerous lengthy experiments. We hypothesize that by taking into consideration the importance of nanoscale quantum phenomena such as confinement and recombination, our developed Python simulation will be able to model the conversion efficiency of CdSe quantum dots in a photovoltaic solar cell with an error of under 5%. Our simulation found CdSe quantum dot conversion efficiency to be 1.66%, which demonstrates comparable rates to the 1.5% efficiency at 50.6% sun found by Lee et. al in 2008 in their experimentation with colloidal CdSe quantum dots– representing a 10.66% realized error and helping prove that simulations can indeed be used as a convincing alternative to painstaking experimentation in the development of optimized quantum dot technologies for energy production. In the future, research should concentrate on reducing this error by factoring in more detailed modeling of quantum phenomenon such as trapping and multiple exciton generation.

INTRODUCTION

The quest for more efficient energy conversion technologies has spurred considerable interest in the development of advanced photovoltaic materials. Among these, quantum dots—nanoscale semiconductor particles—have emerged as a promising alternative to traditional solar cells due to their potential for high conversion efficiencies and tunable electronic properties. Quantum dots, particularly Cadmium Selenide (CdSe), are noteworthy for their size-dependent electronic and optical characteristics. This phenomenon allows quantum dots to absorb and emit light at specific wavelengths, potentially enhancing their performance in photovoltaic applications. However, the experimental process to optimize these materials is both time-consuming and costly, often involving extensive trial and error.

Simulations offer a compelling alternative by enabling researchers to model and predict the performance of quantum dots without the need for exhaustive physical experimentation. Leveraging biophysics equations to simulate the electronic properties and energy conversion efficiency of CdSe quantum dots can significantly expedite the development process. The primary challenge is to accurately account for the nanoscale quantum phenomena, such as quantum confinement and recombination dynamics, that influence the efficiency of these materials. Accurate simulation requires incorporating these complex quantum effects into predictive models to achieve reliable and actionable results. Our research aims to address this challenge by developing a Python-based simulation that models the energy conversion efficiency of CdSe quantum dots in photovoltaic cells. We hypothesize that by incorporating detailed quantum mechanical properties and utilizing biophysics equations, our simulation will be capable of predicting the conversion efficiency with an error margin of less than 5%. This hypothesis is grounded in the assumption that accounting for nanoscale quantum phenomena, such as confinement and recombination rates, will yield a simulation result more closely aligned with experimental data.

The purpose of this study is to validate the accuracy of our simulation model and demonstrate its potential as a tool for optimizing quantum dot-based solar cells. We anticipate that our findings will underscore the viability of simulation as a cost-effective alternative to physical experimentation in the development of advanced photovoltaic technologies. By achieving a simulation accuracy within the proposed error margin, we hope to establish a robust framework for future research and development in quantum dot photovoltaics, ultimately advancing the field towards more efficient and practical solar energy solutions.

RESULTS

Our simulation showed a predicted solar energy conversion efficiency of 1.66% on average for CdSe quantum dots in our system. When comparing our results to similarly unmodified and unoptimized CdSe quantum dots such as the 50% sun efficiency outlined by https://pubs.acs.org/doi/full/10.1021/jp802572b , we get a margin of error of only 10.67%.

Our first set of results pertains to the simulation of varying solar intensities throughout the year. Solar intensity was adjusted for atmospheric effects and focused by the funnel, recorded hourly. As shown in Figure 1, solar intensity peaked around midday and varied significantly based on the zenith angle. The data illustrates a consistent pattern, with higher intensities observed during the summer months and lower intensities during the winter months. The zenith angle reaches its minimum on day 182, corresponding to the summer solstice. Solar intensity is highest around this day but decreases to even lower than day 91 by the time of day 273, indicating that the period following the summer solstice receives the highest solar intensity, aside from the effect of the clearness index.

Figure 2 shows the power output, analyzed for checkpoint days 1, 91, 182, and 273. In the line plot shown in Figure 2a, we see that day 182 exhibited the highest overall power generation. However, at hours 10 and 11, day 91 and day 273 showed higher power output, suggesting variations in weather conditions or the probabilistic quantum effects in the quantum dot system. The results indicate that while solar intensity is a significant factor, it is not the sole determinant of power output. The polynomial curve fit in Figure 2b highlights that day 182 consistently had higher power output, but day 91 was comparable at some points, and day 273 showed greater power output than even day 91 despite a lower solar intensity. This is due to the higher clearness index at day 273. This demonstrates the complex interplay of various factors affecting power output, and the importance of considering all of these various factors. Figure 3, showing the cumulative power output throughout the day for different days, showed that the total energy produced increased steadily, with higher slopes around midday corresponding to the more optimal positioning of the sun. This confirms the influence of solar intensity on cumulative energy production.

Figure 4a provides a visual representation of the temporal and daily variations in power output. It shows that power output peaks between days 169 and 229, corresponding to the summer period with typically sunny days in Austin. Gaps in the heatmap such as those seen on days 94 and 253 indicate periods of high cloudiness, which explains their relatively low power outputs despite the days around them having high power outputs. Figure 4b shows the cumulative power output for each day and highlights the influence of the clearness index. Higher cumulative power outputs correspond to higher clearness index values, emphasizing the importance of this metric in power output calculations, but gaps and unpredictability is also seen, which can be attributed to weather conditions.

Figures 5 and 6 display some of the quantum characteristics of the simulation. Figure 5 shows the size distribution.used for simulating the variations in size commonly found in quantum dots. Employing a logarithmic scale was crucial for correctly modeling the quantum dot array, as it reflects the natural distribution of sizes. We used a lognormal distribution with a mean diameter of 2 nanometers and a standard deviation of 0.4 nanometers. Figure 6 shows a sample electron wavefunction. The wavefunction demonstrates the quantum confinement effects in the quantum dot. The oscillatory nature of the wavefunction and the corresponding probability density peaks illustrate the discrete energy levels and the spatial confinement of the electron. The probability density is higher near the center of the quantum dot and decreases towards the edges, indicating that the electron is more likely to be found near the center.

DISCUSSION

The primary results indicate that our simulation effectively models the conversion efficiency of CdSe quantum dots with a realized error of 10.66%. The variations in solar intensity throughout the year, as shown in Figure 1, demonstrate the importance of considering seasonal and daily changes in solar exposure when designing photovoltaic systems. The power output results, especially those depicted in Figures 2 and 3, highlight the complexity of factors influencing energy production, such as weather conditions and quantum effects.

The cumulative power output data (Figure 4) emphasize the impact of clearness index and atmospheric conditions on overall power generation. Figures 5 and 6 provide insights into the quantum mechanical behavior of the quantum dots, including the size distribution and wavefunction characteristics, which are crucial for understanding their energy conversion properties.

Several factors could have influenced our results. One significant limitation is the accuracy of our atmospheric data, which directly impacts the calculated solar intensity and, consequently, the power output. Additionally, the simplifications made in modeling quantum mechanical processes, such as assuming certain quantum numbers and ignoring some complex interactions, could have introduced errors.

The biggest error we have to acknowledge is inaccurate or missing data parameters vital to ensuring the maximum accuracy of our simulation. Since values such as that of the trapping coefficient for CdSe quantum dots are not readily available, we have to manually approximate the value, which introduces significant deviations from the real values.

Future research should be aimed at utilizing the most optimal parameters in these simulations, which would ensure that the simulation matches reality much more closely. Moreover, optimization scripts could be incorporated to understand the ideal parameter to use for a quantum dot, which could influence the processes used to create the quantum dot in the experiment.

In conclusion, our simulation of CdSe quantum dots demonstrated a conversion efficiency comparable to experimental results, validating the potential of simulation as a tool for optimizing quantum dot technologies. By addressing the limitations and exploring new avenues of research, we can further enhance the efficiency and practicality of quantum dots in solar energy applications.

MATERIALS AND METHODS

To accurately simulate the intake of sunlight, we begin by calculating the zenith angle, which is crucial for understanding the interaction of sunlight with our system. The zenith angle, denoted as θ_z, is the angle between the vertical direction and the line to the sun. For our location in Austin, Texas, θ_z is given by:

$$\theta_z = \cos^{-1}(\sin(\delta)\sin(\varphi)+\cos(\delta)\cos(\varphi)\cos(H)) \quad (1)$$

where δ is the solar declination, φ is the latitude of Austin, and H is the solar hour angle. These parameters vary with time and date and are essential for calculating the precise position of the sun in the sky. δ and H are found from formulae given by NOAA. We then took the cosine of this angle and multiplied it by the solar constant (approximately 1361W/m2) to find the adjusted solar intensity. If $\cos(\theta_z)$ is not positive, this adjusted quantity just becomes equal to 0 as the sun is beneath the horizon at that time.

We now need to correct the sunlight intensity value based on the atmosphere. We use the clearness index, for which values will be sourced from NASA's Atmospheric Science Data Center and applied to the adjusted intensity on an hourly basis, ensuring a dynamic adaptation to atmospheric conditions. By multiplying our adjusted intensity with this factor, we get the true value of solar intensity that hits the ground on any given day.

The funnel's hyperbolic shape is modeled to focus the incoming solar radiation onto the quantum dot array. The reflective properties of the polished aluminum funnel are crucial here. The concentration factor is calculated based on the funnel's geometry, specifically the ratio of the cross-sectional area of the funnel's wider end to that of the narrower end focused on the quantum dot array. Using this factor and the reflective percentage of polished aluminum, we see that I_{focus} is equal to the product of the reflectivity of polished aluminum (83%), the intensity after atmospheric adjustments, and the concentration factor of 2500 (accounting for the aperture radii of 50 and 1 centimeters, respectively).

We calculate the energy per photon using Planck's equation, using the average photon wavelength of 550 nm. This is done by the equation $E_{photon} = \frac{hc}{\lambda}$. With the total intensity and the energy per photon, we can calculate the number of photons per second striking a area as the product between I_{total} and area divided by E_{photon}. Finally, we obtain the photon generation rate per hour by multiplying the previous value by a factor of 3600. This rate is a crucial input metric for the next part of our simulation, the quantum dot array. To model quantum dots and excitons accurately, we must consider as many major properties and processes as possible, including material composition, geometric structure, quantum mechanical properties, and size dependent properties. This ensures that we calculate the exciton generation rate as accurately as possible. The chosen material for our quantum dots is Cadmium Selenide (CdSe), known for its high absorption efficiency. The distribution of quantum dot sizes is typically characterized by a lognormal distribution, where D(d) is the probability density for diameters, $\mu = \ln(3.9\times10^{-9})$ represents the mean logarithm of the diameters, and $\sigma = 0.4$ is the standard deviation of the logarithm of the diameters. The distribution will range from 2.3 to 5.5 nanometers. To properly simulate the characteristics of excitons and calculate the rate at which excitons transition between energy states, we numerically solve the Schr¨odinger equation for a 3D finite potential well. The finite difference method is employed using a grid size of 25 and a step size governed by the radius divided by the grid size. This provides the energy levels of our dot and wavefunctions for electrons and holes. The Laplacian operator ∇^2 of the Schrödinger equation is discretized using the central difference method. General wavefunctions for electrons (ψ_e) and holes (ψ_h) in an ellipsoidal quantum dot with a 3D finite potential well can be approximated as:

$$\psi_e(r) \approx \sum_{n,l,m} A^{e}_{n,l,m} R^{e}_{n,l}(r) Y^{l}_{m}(\theta, \varphi) u_{CB}(r)$$

$$\psi_h(r) \approx \sum_{n,l,m} A^{h}_{n,l,m} R^{h}_{n,l}(r) Y^{l}_{m}(\theta, \varphi) u_{VB}(r)$$

where r denotes the position vector in ellipsoidal coordinates, n, l, m are quantum numbers, $A^{e/h}_{n,l,m}$ are n,l,m normalization constants, $R^{e/h}_{n,l}(r)$ are the radial functions obtained numerically, $Y^{l}_{m}(\theta, \varphi)$ are spherical harmonics, and $u_{CB/VB}(r)$ are the Bloch functions' periodic parts for the conduction and valence bands. The normalization constant is calculated by through the normalization principle, that the total integral of the absolute square of the wavefunction over all space must always be 1. The radial functions are obtained through the magnitude of the wavefunction solutions of the Schrödinger equation, calculated numerically by solving the discretized Schrödinger equation in the finite potential well. The spherical harmonics describe the angular part of the wavefunction. For simplicity, we assume the quantum numbers l and m are 0. The Bloch functions describe the periodic part of the wavefunction in the crystal lattice for the conduction and valence bands, respectively. They are calculated using Bloch's theorem.

3.3 Quantum Confinement Effects and Transition Rate

Quantum confinement significantly alters the electronic properties of quantum dots. The effective bandgap energy E_{gap} is modified due to the spatial confinement of charge carriers and can be expressed as:

$$E_{gap} = E_{bulk,gap} + \frac{\hbar^2 \pi^2}{2\mu d^2} - \frac{1.8e^2}{4\pi\epsilon\epsilon_0 d}$$

where $E_{bulk,gap}$ is the bulk bandgap energy, d is the quantum dot diameter, and μ is the reduced mass of the electron-hole pair. The dipole matrix element, essential for calculating transition rates, is determined by the overlap of the initial and final state wavefunctions. This matrix element is then used in Fermi's Golden Rule to calculate the transition rate between states. The rate at which excitons are generated by photon absorption is the product of the photon generation rate, the quantum efficiency, and the transition rate. These factors collectively determine the efficiency of exciton creation within the quantum dot system. Exciton recombination, dissociation, migration, and trapping rates are critical to determining the overall exciton density. The primary processes considered include recombination rate(The rate at which excitons recombine typically proportional to the square of the exciton density), dissociation rate(the rate at which excitons dissociate into free carriers, influenced by the binding energy and temperature), migration rate(The rate at which excitons move within the quantum dot), trapping rate(The rate at which excitons are trapped at defects or other localized states), and thermal dissociation rate(The rate at which excitons dissociate due to thermal energy). The probability of

Multiple Exciton Generation (MEG) occurs when the photon energy exceeds a thresh- old, typically 2-3 times the bandgap energy. The rate of Auger recombination, a non-radiative process, is proportional to the cube of the exciton density. Additionally, biexciton formation and recombination are considered, where biexciton formation is influenced by the biexciton binding energy and temperature. The overall exciton density, $n_{exciton}$, considers both generation and loss mechanisms:

$$n_{exciton} = \frac{\Gamma_{gen} \cdot (1 + P_{MEG})}{\Gamma_{recomb} + \Gamma_{trap} + \Gamma_{thermal} + \Gamma_{Auger} + \Gamma_{biexciton}}$$

where Γ_x represents the rate value of the process x. The net exciton generation rate that reaches the conversion area, accounting for various processes, is calculated as:

$$\Gamma_{net} = (\Gamma_{abs} \cdot \eta_{QE} \cdot E_{exciton}) + \Gamma_{dissoc} - \Gamma_{recomb} + \Gamma_{migrate} - \Gamma_{trap} + \Gamma_{thermal}$$

This rate, along with the exciton density, directly relates to the overall energy production and efficiency of a quantum dot system. The efficiency and performance of a quantum dot photovoltaic system can be evaluated by calculating the power and energy output. This involves determining the photocurrent generated by excitons, the resultant power output, and the total energy output over a specified time interval. The photocurrent, Iphoto, is generated by the movement of charge carriers (excitons) in response to light absorption. It is calculated as: $I_{photo} = e \cdot \Gamma_{exciton} \cdot A$, where e is the elementary charge, $\Gamma_{exciton}$ is the exciton generation rate, A is the area of the quantum dot photovoltaic cell. The power output, P_{output}, is the product of the photocurrent and the voltage across the cell. The total energy output, Eoutput, over a given time interval is obtained by multiplying the power output by the duration of the interval.

FIGURES AND FIGURE CAPTIONS

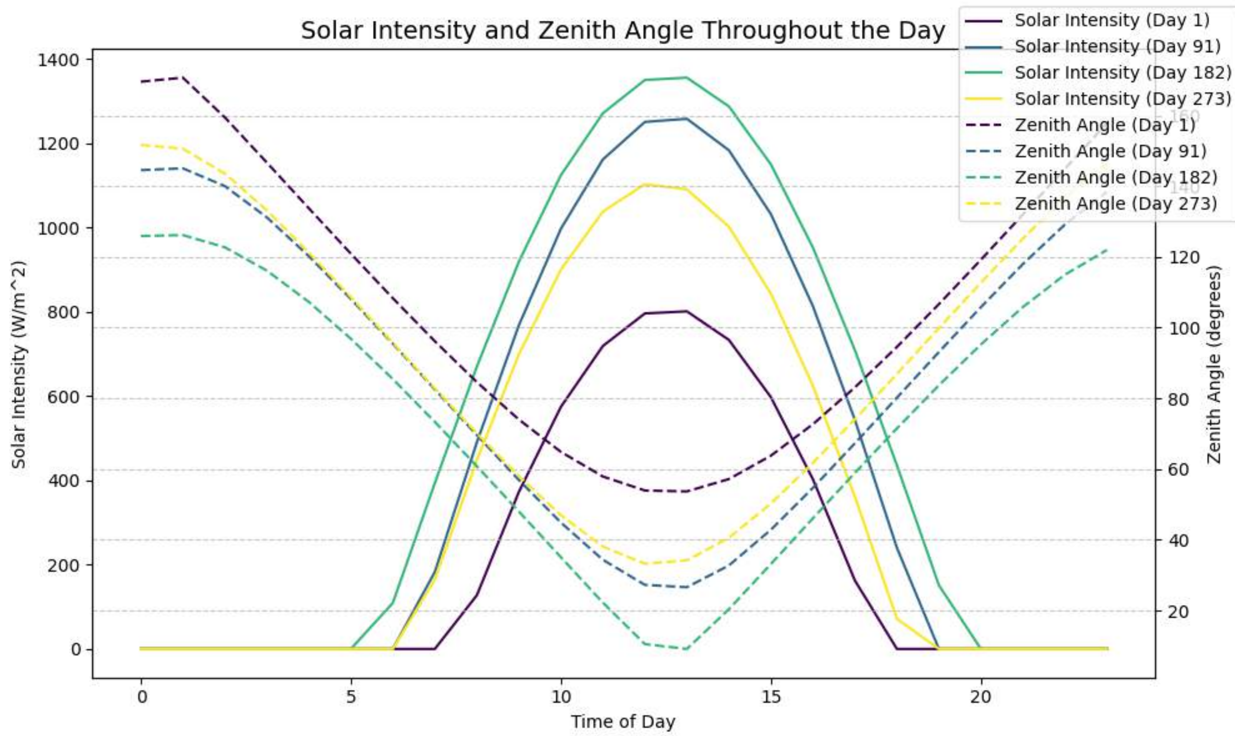

Figure 1. Solar Intensity and Zenith Angle Plot Over A Day. Line plot shows the variation in solar intensity and zenith angle for four days, chosen to represent quarters of the year. The dotted lines indicate zenith angles and the solid indicate solar intensity.

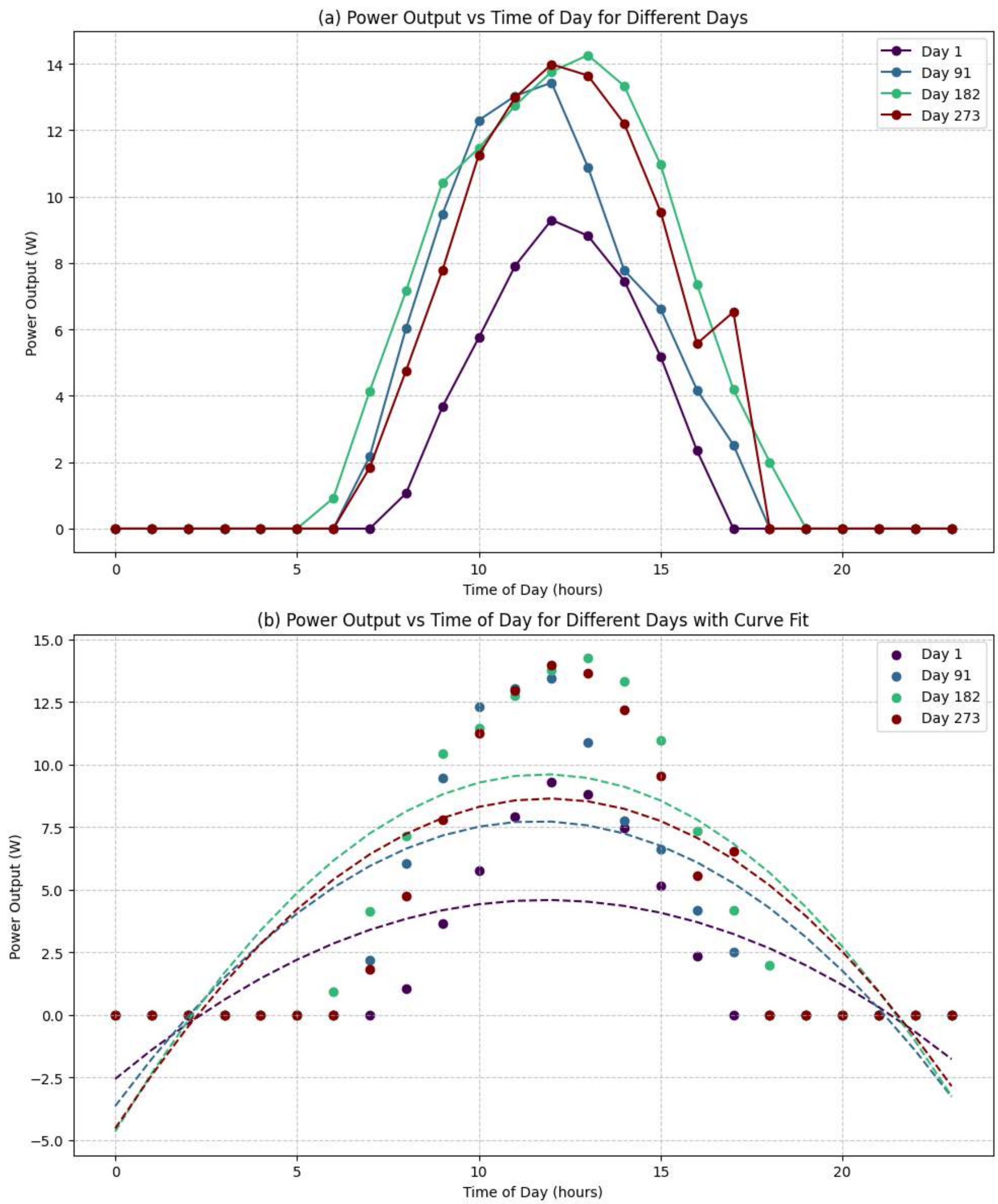

Figure 2. Power Output vs Time of Day for Different Days. (a) This plot shows how the power output changes over the course of 4 different selected days. It adapts a line fit of the data, which allows us to see the changes in power of various graphs at different hours. The individual dots are the true power outputs for a given hour and day. **(b)** This plot is similar to **(a)**, but uses a curve fit. This allows us to discern more general trends about how the power output progresses over a day.

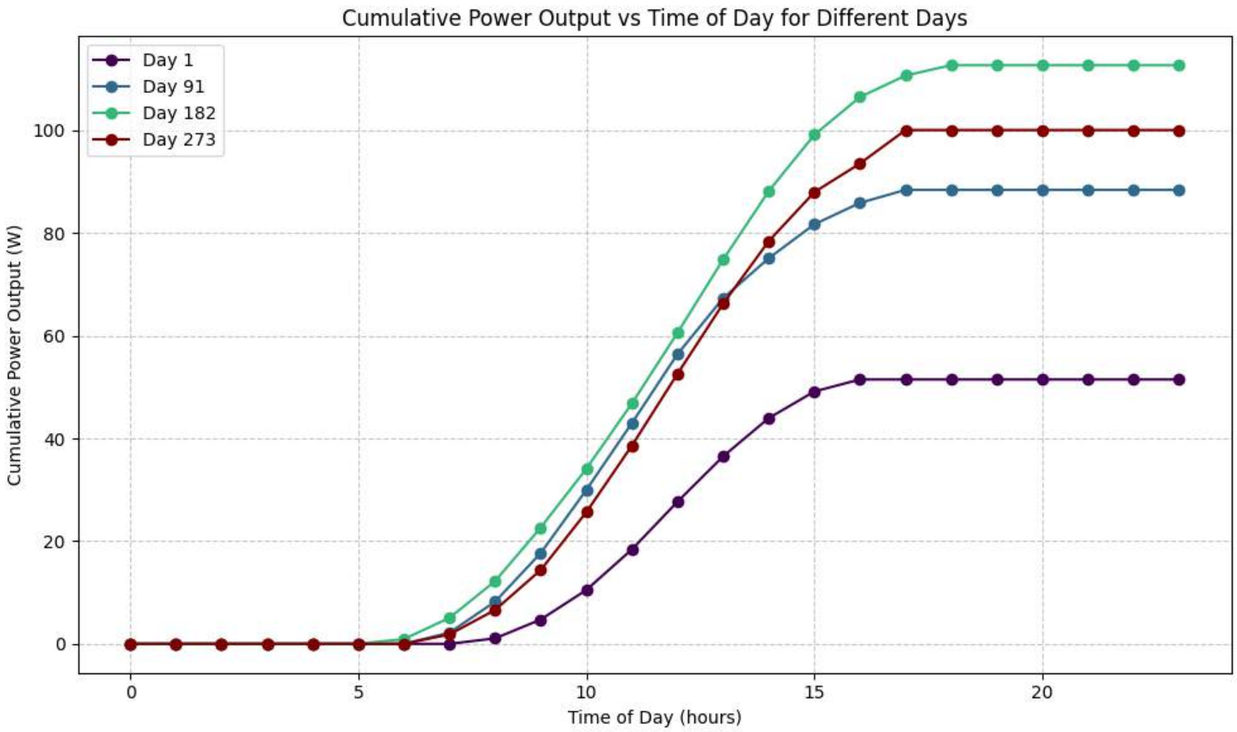

Figure 3. Cumulative Power Output vs Time for Different Days. Line plot showing the cumulative power output over the course of four selected days. This plot shows when power starts being generated, the slopes show when it is at maximum generation, and when power output stops over the period of a day.

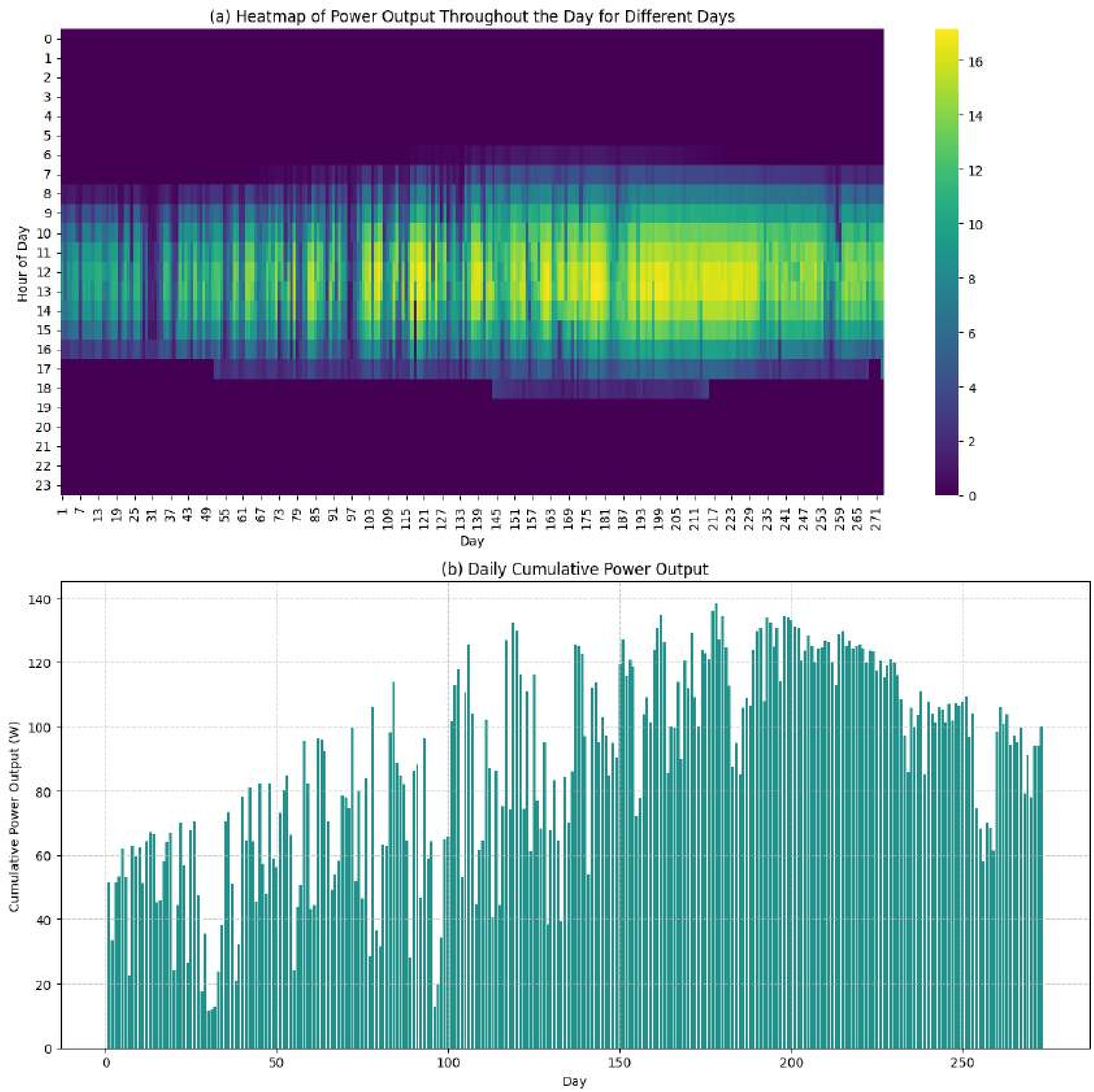

Figure 4. Daily Cumulative Power Output. (a) Heatmap of the predicted power outputs from January 1st to September 30th. The heat varies over a day, allowing us to see the patterns in power outputs for a given hour over our date range. **(b)** This plot shows the cumulative power output for every day in the year.

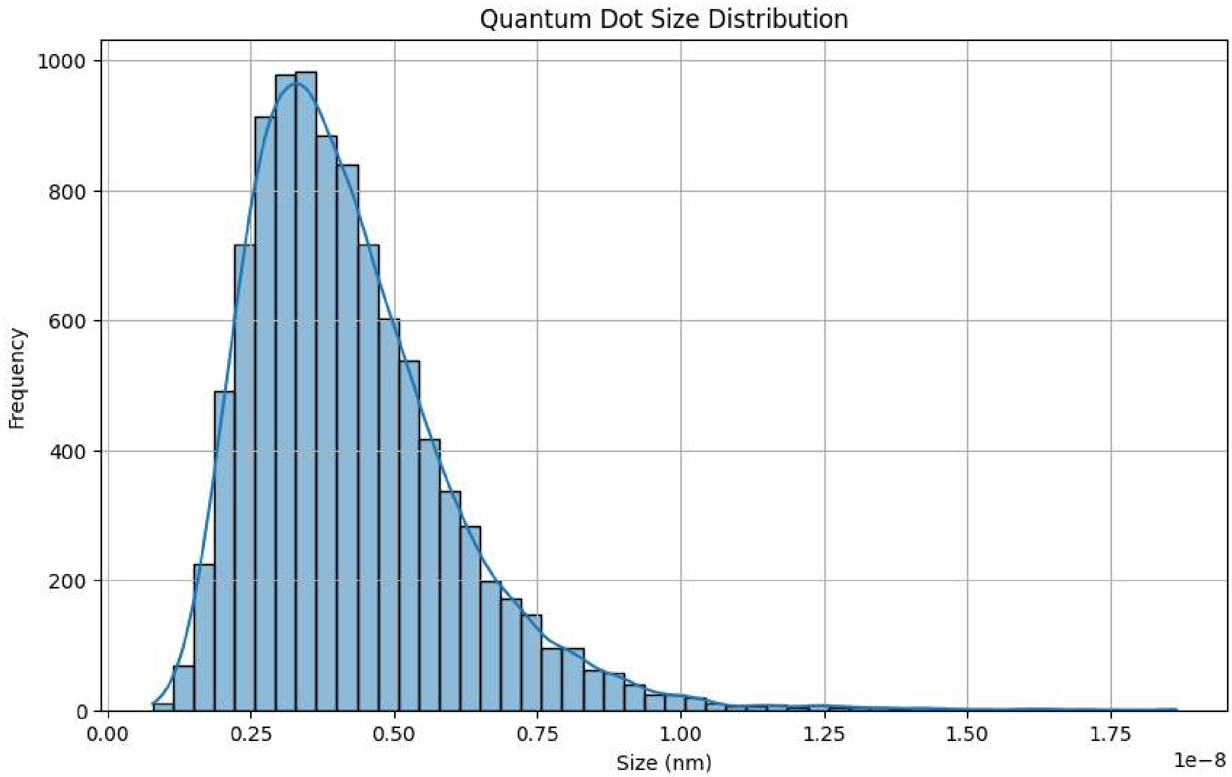

Figure 5. Quantum Dot Size Distribution. Shows the distribution of quantum dot sizes in our simulation. The curve represents the function for CdSe quantum dots, and the frequency histogram helps identify where the sizes are focused. The distribution is lognormal.

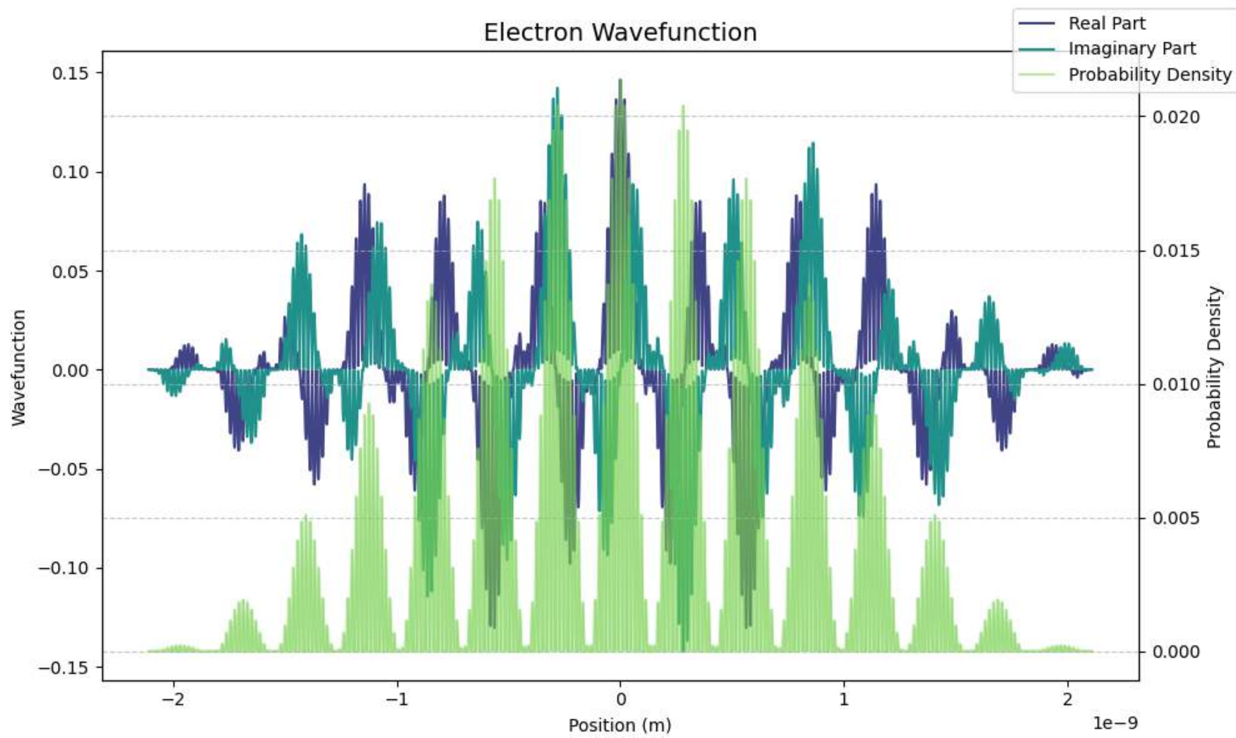

Figure 6. Example Electron Wavefunction. Shows the real and imaginary parts of the wavefunction, as well as the probability density. The real part of the wavefunction exhibits an oscillatory pattern, characteristic of the particle's quantum state. Nodes, where the wave function crosses zero, indicate points of zero probability density, and the symmetry suggests the potential well's shape and the particle's energy state. The imaginary part complements the real part, providing critical phase information essential for understanding phenomena like interference and tunneling. The probability density, represented by the squared magnitude of the wavefunction, shows the likelihood of finding the particle at different positions. Higher probability density areas indicate where the particle is most likely confined, while the spreading of the wavefunction gives insights into the degree of quantum confinement.

APPENDIX

Code and required dependencies are included in a separate file.